Available online at www.sciencedirect.com

ScienceDirect

Acta Materialia 82 (2015) 266–274

Acta MATERIALIA

www.elsevier.com/locate/actamat

# Hydrogen diffusivities as a measure of relative dislocation densities in palladium and increase of the density by plastic deformation in the presence of dissolved hydrogen

Martin Deutges,[a,*] Hans Peter Barth,[a] Yuzeng Chen,[b] Christine Borchers[a] and Reiner Kirchheim[a,c]

[a] *Institut für Materialphysik, Georg-August-Universität Göttingen, Friedrich-Hund-Platz 1, 37077 Göttingen, Germany*
[b] *State Key Lab of Solidification Processing, Northwestern Polytechnical University, Xián, People's Republic of China*
[c] *International Institute for Carbon-Neutral Energy Research (WPI-I²CNER), Kyushu University, Japan*

Received 27 May 2014; revised 3 September 2014; accepted 4 September 2014
Available online 4 October 2014

**Abstract**—The effect of dissolved hydrogen on the dislocation density in cold-rolled palladium was investigated in order to provide evidence of a line energy reduction caused by hydrogen–dislocation interaction as proposed by the defactant concept. For this issue, palladium samples were electrochemically charged with hydrogen and subsequently cold rolled. Using conventional methods (X-ray diffraction, transmission electron microscopy) and a newly developed diffusion method, it was shown that the dislocation density after deformation increases with increasing hydrogen concentration.


*Keywords:* Palladium; Hydrogen embrittlement; Plastic deformation; Dislocation density; Diffusion

## 1. Introduction

A wide range of effects can be attributed to the presence of hydrogen in metals. For instance, dissolved hydrogen can enhance crack propagation [1] or lead to the formation of blisters on surfaces [2]. In the microscopic range, hydrogen can interact with all types of defects. In many metals hydrogen has a large influence on the formation and stabilization of vacancies, e.g. in Al [3], Nb [4] and Pd [5]. This is explained by a decrease in the formation energy of vacancies due to the segregation of hydrogen atoms to these vacancies [6,7].

Another effect is a transition from ductile to brittle behavior by the introduction of hydrogen into e.g. Al [8] or austenitic stainless steels [9,10]. One explanation for this effect is the enhanced mobility of dislocations due to the segregation of hydrogen to these dislocations [1,11].

The influence of hydrogen on dislocations is discussed in both an earlier report by Chen et al. [12] and this report. It will be shown that the line energy of dislocations is decreased by charging palladium with hydrogen, which in turn leads to an increase in dislocation density during cold deformation.

These effects can be explained by the defactant concept [6,7,13], the basis of which is that a decrease in the overall free energy caused by a segregation of solute atoms to the neighborhood of defects can be ascribed to a decrease in the defect formation energy. This is an alternative point of view compared to textbook concepts, according to which solute atoms migrate to defects because their energy of solution is decreased.

In this study the effect of hydrogen on the density and arrangement of dislocations in cold-rolled palladium–hydrogen alloys was investigated. Due to the high solubility of hydrogen (up to $1.0 \times 10^{-2} \frac{H}{Pd}$ at 298 K [14]) in the α-phase of the palladium–hydrogen system, this system was chosen as a model system.

For this purpose, well-annealed polycrystalline palladium samples were electrochemically alloyed with hydrogen and subsequently cold rolled. The dislocation densities of the cold-rolled samples were estimated via two different methods: a conventional Williamson and Hall method [15] and a newly developed pulse diffusion method.

## 2. Theory

### 2.1. The interaction between solute atoms and crystal defects – the defactant concept

Solute atoms in solid material segregate to defects like vacancies [16], dislocations [17] or grain boundaries [18].

* Corresponding author at: Institut für Materialphysik, Georg-August-Universität Göttingen, Friedrich-Hund-Platz 1, 37077 Göttingen, Germany; e-mail: mdeutges@ump.gwdg.de

http://dx.doi.org/10.1016/j.actamat.2014.09.013
1359-6462/

This phenomenon can be described in analogy to the segregation of surfactants to surfaces described by the well-known theory of Gibbs [19]. The defactant concept regards the surface as a crystal defect like any other internal defect. Therefore the relation of the reduction of the surface energy $\gamma$ with the chemical potential of the solute $\mu$ provided by Gibbs can also be used to describe internal crystal defects [6,7]:

$$d\gamma = -\Gamma d\mu \quad (1)$$

Of key interest is the excess $\Gamma$, which represents the excess amount of segregated solute atoms to the defect surface in relation to the concentration of the solute atoms in a defect-free part of the material.

In the case of dislocations, solute atoms will enrich around the core of dislocations, thus dislocations have a positive excess $\Gamma$. Due to the stress field of a dislocation, interstitial lattice sites beneath the glide plane of an edge dislocation are expanded. This causes solute atoms to segregate to dislocations if they expand the lattice, otherwise they segregate to sites above the glide plane.

The positive excess of solute at dislocations then reduces the formation energy of dislocations when the chemical potential of the solute is increased, as described quantitatively by Eq. (1). The dependency of the formation energy of a defect with increasing chemical potential is shown schematically in Fig. 1. At low chemical potentials, only few solute atoms interact with the defect, leading to $\Gamma = 0$. With increasing chemical potential, the excess $\Gamma$ increases. When the excess saturates, a constant slope can be expected (line 1), whereas line 2 shows the behavior when the excess does not saturate but increases with increasing $\mu$. When a new phase nucleates (line 3), the defect energy does not decrease with increasing solute concentration any more because of the constant chemical potential during the phase transition.

### 2.2. Dislocation dynamics in the context of the defactant concept

Direct observations of the motion of dislocations in an environmental transmission electron microscopy (TEM) during straining experiments in a hydrogen atmosphere

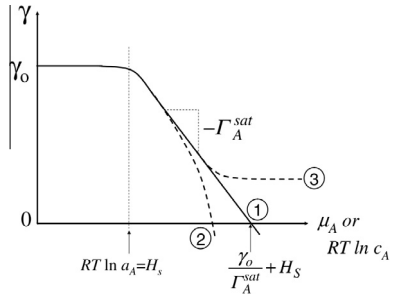


**Fig. 1.** Schematic representation of the course of the formation energy $\gamma$ with increasing chemical potential $\mu$. At low chemical potentials, the effect of solute atoms to the defect can be ignored. With increasing chemical potential, the excess $\Gamma$ increases. When the excess saturates, a constant slope can be expected (line 1), whereas line 2 shows the behavior when the excess does not saturate but increases with increasing $\mu$. When a new phase nucleates (line 3), the defect energy does not decrease with increasing solute concentration any more because of the constant chemical potential during the phase transition. Adopted from Refs. [6,7].

[20,21] show that the dislocation mobility is enhanced when hydrogen is present. Furthermore, it is shown that the interaction between dislocations as well as between dislocations and other obstacles [17] is diminished. This is explained by a hydrogen shielding model [22].

The defactant concept provides a different explanation of the enhanced dislocation velocity in the presence of hydrogen. Because dislocations move by the formation of kink pairs, the required defect formation energy is reduced by the presence of the defactant hydrogen. When kink pair nucleation is the rate-controlling step for dislocation motion, such a reduction in kink formation energy will lead to softening [7].

Two other defect–solute interactions can contribute to the increase in dislocation mobility: due to solute atoms, the formation energy of vacancies is changed, and for positive excess solute the formation energy is reduced [6,7]. Thus climbing of edge dislocations over obstacles can be eased. Another effect is that the interaction of dislocations on different glide planes is affected. When one dislocation cuts another dislocation on a different glide plane, kinks or jogs are introduced into the dislocations [23, chap. 22]. The ease of the formation of kinks leads to a reduction in the interaction energy between dislocations, which allows dislocations to rearrange more easily. This leads to higher local dislocation densities. Fluctuations in the density allow the formation of dislocation cells, as described by Holt et al. [24,25] in a model where the cell formation is handled like spinodal decomposition. Furthermore, the number of dislocations affected by a moving dislocation is increased. This means that the correlation length of the dislocations is increased, which, according to Hähner [26], leads to larger dislocation cells with more densely populated cell walls.

## 3. Experimental details

A 500 $\mu$m thick palladium sheet of 99.95% purity supplied by Wieland Edelmetalle GmbH was used for the investigation. Pieces of $6 \times 20$ mm$^2$ were cut by spark erosion. The palladium pieces were annealed at 1172 K in a vacuum furnace at $10^{-6}$ mbar for 48 h and subsequently furnace cooled for 24 h to prevent residual stress in the samples.

The samples were charged electrochemically with hydrogen using an electrolyte composed of $H_3PO_4$ and glycerine (1:2 by volume). By using a maximum current density of 0.3 mA cm$^{-2}$, the entire hydrogen created by the electrolysis process is dissolved in the palladium, i.e. no hydrogen bubbles are observed. The hydrogen concentration $c_H$, which is the molar fraction of the number of hydrogen atoms to palladium atoms, can be determined via Faraday's law:

$$\Delta c_H = \frac{It}{n_{Pd}F}, \quad (2)$$

where $t$ is the time of the loading process, $F$ is Faraday's constant, $I$ is the total current and $n_{Pd}$ is the amount of palladium.

Immediately after loading with hydrogen, the samples were cold rolled to a thickness reduction of $(50 \pm 3)$%.

TEM specimens were prepared by electropolishing using a Tenupol-2 electropolisher with an electrolyte composed of 70 vol.% acetic acid (96%) and 30 vol.% perchloric acid (60%) at 287 K and a voltage of 10 V against a Pt counter electrode.

A Philips CM12 conventional scanning transmission electron microscope operating at 120 kV was used to investigate the TEM samples.

The dislocation density was estimated via two different methods: with a conventional Williamson and Hall method [15] and by a newly developed diffusion method.

### 3.1. Measuring the dislocation density by the method of Williamson and Hall

Many defect analysis techniques [27–29] using X-ray diffraction (XRD) are based on the method originally developed by Williamson and Hall [15]. The aim of this method was to calculate the internal strain $\epsilon$ and the grain size $D$ of uniformly deformed materials by using XRD patterns.

Assuming that only the broadening related to the grain size $\beta_D$ and the broadening related to the strain $\beta_\epsilon$ contribute to the broadening of the peaks in an XRD pattern, the full width at half maximum of Lorenzian-shaped peaks $\beta$ is the sum of the different contributions:

$$\beta = \beta_D + \beta_\epsilon + \beta_{inst} \tag{3}$$

The broadening of the instrument $\beta_{inst}$ can be measured separately using unstrained Si powder and is interpolated for the angular peak position $\theta$. The relation of the broadening of a peak to the grain size and the strain is [15]:

$$\begin{aligned}\beta - \beta_{inst} &= \frac{\lambda}{D\cos\theta} + 2\epsilon\tan\theta \Rightarrow \cos\theta(\beta - \beta_{inst}) \\ &= \frac{\lambda}{D} + 2\epsilon\sin\theta\end{aligned} \tag{4}$$

The measured peak widths can be plotted according to this formula. Using a linear fit, $\epsilon$ and $D$ can be acquired from the slope and the $y$-intercept using the X-ray wavelength $\lambda$. Assuming that the internal strain is generated only by dislocations, the dislocation density $\rho$ can be calculated from $\epsilon$ [30]:

$$\rho = k\frac{\epsilon^2}{b^2} \tag{5}$$

where $b$ is the Burgers vector and $k$ is a geometrical constant, with $k = 16.1$ for face-centered cubic materials and $k = 14.4$ for body-centered cubic materials [30].

In this study, the XRD measurements were carried out using a Philips X'pert MRD diffractometer operating with Co $K_\alpha$ radiation with a wavelength $\lambda_{K\alpha 1} = 0.178897$ nm. The step size and counting time per step were 0.02° and 20 s, respectively. The instrumental broadening profile was obtained by measuring a standard strain-free Si powder.

Prior to the measurement, residual hydrogen was removed from the samples by uncharging it in a double cell with a constant potential of 0.78 V against a Pt counter electrode until the electrical current in the circuit was below 1 $\mu$A. Since the average grain size of the cold-rolled Pd–H alloys is not smaller than 100 $\mu$m according to light microscopy micrographs (not shown), the contribution of the crystallite size to the Bragg peak broadening is considered to be negligible and the term $\frac{\lambda}{D}$ in Eq. (4) is set to zero. Performing a linear-least-squares fit on the measured data shown in Fig. 2 and setting the intercept of the ordinate to zero, the lattice strain $\epsilon$ of the metal can be derived by taking the slope of the fitted line.

### 3.2. Measuring the dislocation density by diffusion of hydrogen

A laboratory-made electrolytic double-cell set-up (see Fig. 3) is used to measure the diffusion coefficient of hydrogen in palladium and the trapped hydrogen at lattice defects.

An electrolytic double cell combines two different electrochemical experiments. The so-called loading side is equipped with a Pt counter electrode and is used to load hydrogen into the sample, which is mounted between the two half cells. The other side of the Pd sample is called the measuring side, and is used to measure the voltage $U$ between the sample and an Ag–AgCl reference cathode in order to acquire the electromotive force (EMF) of the corresponding half cell. The whole set-up can be cooled. A broad overview of different measuring methods with a double-cell set-up is given in Ref. [31].

Both cells are filled with an electrolyte composed of $H_3PO_4$ and glycerine (1:2 by volume). The electrolyte was bubbled with argon gas for 24 h to remove dissolved oxygen.

To ensure that no residual hydrogen remained in the samples after cold rolling, the samples were uncharged in the double cell with a constant potential of 0.78 V against a Pt counter electrode, until the electrical current in the circuit was below 1 $\mu$A. To load palladium with hydrogen, the Pt counter electrode and the specimen are connected to a direct electric current source and a relay is used to discontinue the loading.

In order to measure the diffusion coefficient of hydrogen in palladium, hydrogen is loaded for 1000 ms at a constant current and the EMF is measured afterwards. The electric

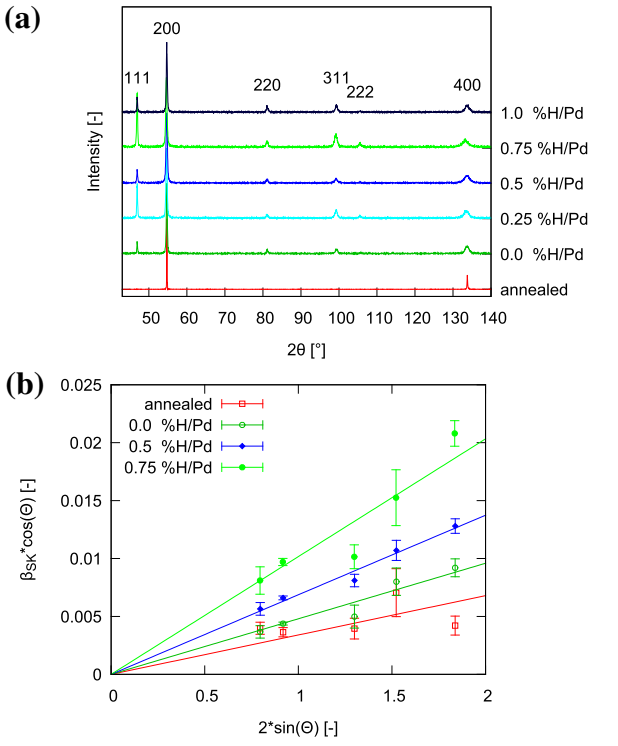


**Fig. 2.** Examples of the measured XRD profiles (a) of the cold-rolled Pd–H alloys with different H/Pd ratios and well-annealed Pd, and (b) Williamson–Hall plots for those diffraction patterns (see also Ref. [12]).

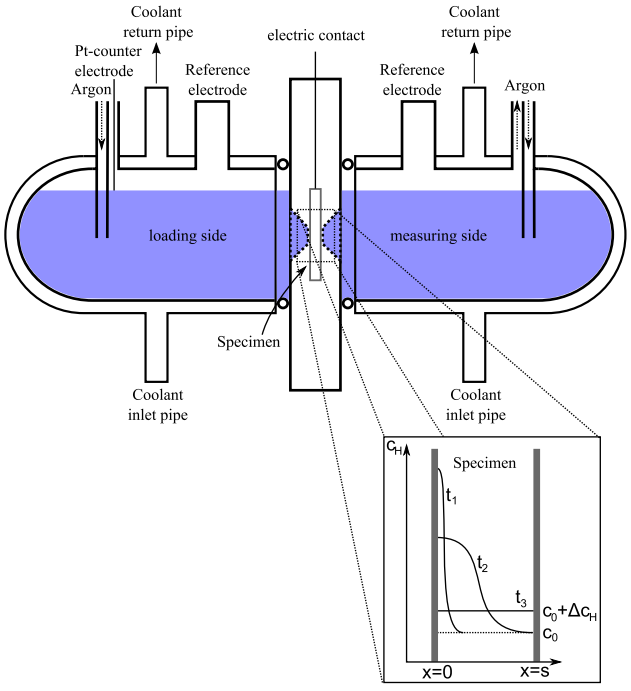


**Fig. 3.** Schematic presentation of the double-cell set-up used in this study. The left cell is used to dissolve hydrogen electrochemically in the palladium and is called the loading side. The right cell is used to measure the EMF and thus the chemical potential of hydrogen at the surface of the specimen. The inset schematically shows the distribution of hydrogen shortly after the pulse was initialized ($t_1$), at an intermediate stage ($t_2$) and after a new constant concentration level $c_0 + \Delta c$ is reached ($t_3$). A detailed discussion of the transient concentration profiles is given in Ref. [32].

current density is set to 0.3 mAcm$^{-2}$ at the beginning of the experiment and is increased at higher hydrogen concentrations up to 30 mAcm$^{-2}$, which is possible without the emergence of hydrogen bubbles for short loading times. When hydrogen is uniformly distributed, the EMF will be constant and a new loading cycle will be started.

In the following, the relation of the EMF to the diffusion coefficient and the trapped hydrogen is derived according to Ref. [33,34].

At thermodynamic equilibrium, the EMF measured as voltage $U$ between the sample and an Ag–AgCl reference cathode is related to the chemical potential of hydrogen at the surface of the sample

$$U = U_0 + \frac{\mu_H}{F}, \tag{6}$$

$U_0$ is the reference potential difference between the reference cathode and the sample for standard conditions, i.e. $T = 295$ K and hydrogen pressure of 1 bar. By definition, the chemical potential of dissolved hydrogen is related to its thermodynamic activity $a_H$:

$$\mu_H = \mu_H^0 + RT\ln(a_H), \tag{7}$$

$$= \mu_H^0 + RT\ln(\gamma c_H) \tag{8}$$

The activity $a_H$ can be expressed as the product of the activity coefficient $\gamma$ and the hydrogen concentration $c_H$. In the case of a dilute solution, the activity coefficient is independent of concentration.

The development of the EMF with time allows the tracer diffusion coefficient $D_H$ of hydrogen in palladium to be determined. Therefore, Fick's first and second laws (Eq. (9)) have to be solved for this experimental set-up. The aim of the following derivation is to establish an expression for the change of the hydrogen concentration $\Delta c_H$ on the measuring side ($x = s, s$: sample thickness) with time $t$ after the charging pulse is initialized.

$$j = -\widetilde{D_H}\frac{\partial c_H}{\partial x} \tag{9}$$

$$\frac{\partial c_H}{\partial t} = \widetilde{D_H}\frac{\partial^2 c_H}{\partial x^2} \tag{10}$$

The driving force for the particle flux $j$ is the result of a spatial ($x$) gradient of the hydrogen concentration $c_H$ or, more precisely, a gradient of the chemical potential $\mu_H$ of hydrogen in palladium. $\widetilde{D_H}$ is the chemical diffusion coefficient. To solve Fick's laws, the following boundary and initial conditions are used to describe the experimental set-up (see also [32]):

$$c_H(x, t = 0) = c_0 \tag{11}$$

At $x = 0$ a current pulse is imposed for $0 \leqslant t \leqslant t_p$, after which open circuit conditions with $j = 0$ apply:

$$-\widetilde{D_H}\frac{\partial c_H}{\partial x}\bigg|_{x=0} = \begin{cases} I & \text{for } 0 \leqslant t \leqslant t_p \\ 0 & \text{for } t > t_p \end{cases} \tag{12}$$

Open circuit conditions also apply at $x = s$ after the current pulse:

$$-\widetilde{D_H}\frac{\partial c_H}{\partial x}\bigg|_{x=s} = 0 \tag{13}$$

At the starting time $t = 0$, hydrogen dissolved by previous charging cycles in the sample $c_0$ is distributed uniformly in the sample (Eq. (11)).

The particle flux $j$ in Eqs. (9) and (12) can be expressed by Faraday's law (Eq. (2)) when the current $I(t)$ is small. This means that every hydrogen ion which is split by the electrolysis process on the surface of the sample $A$ diffuses into the sample. The loading time in this study is $t_p = 1$ s, which is much shorter than the diffusion time through the sample. With these conditions, Fick's laws can be solved for the hydrogen concentration at the measuring side for $t > 0$ with $\Delta c_H$ the concentration change of the whole sample due to the pulse [35]:

$$c_H(x = s, t) \approx c_0 + \Delta c_H + \Delta c_H \sum_{n=1}^{\infty} 2(-1)^n \exp\left(-\frac{n^2\pi^2 \widetilde{D_H} t}{s^2}\right) \tag{14}$$

For small times ($t \to 0$), the changes of concentration are small and the EMF does not change. The corresponding EMF vs. time curve is a horizontal straight line, which is called the baseline. For $t \approx s^2/\widetilde{D_H}/20$, appreciable amounts of hydrogen diffuse through the sample and change the EMF at the measuring side ($x = s$). After homogenization for $t \gg s^2/\widetilde{D_H}$, the concentration gradient vanishes and the EMF vs. time curve becomes a horizontal straight line again, which will be the new baseline for the following current pulse (see Fig. 4). The diffusion coefficient can be determined from a so-called breakthrough time $t_{\widetilde{D}}$, defined as the intersection of the tangent through the point

of inflection and the baseline [36] (see Fig. 4). The following expression for $t_{\mathrm{D}}^{\sim}$ was derived [32,36] drom the analytical solution Eq. (14):

$$t_{\mathrm{D}}^{\sim} = K \times \frac{s^2}{\widetilde{D_{\mathrm{H}}}} \tag{15}$$

Here, $K$ is numerical constant which has the value $K = \left(\frac{5}{2} - \sqrt{6}\right)$ for the chosen boundary conditions (Eqs. (11)–(13)).

The tracer diffusion coefficient $D_{\mathrm{H}}$ of hydrogen in palladium can be calculated using the Darken equation:

$$D_{\mathrm{H}} = \widetilde{D_{\mathrm{H}}}\left(1 + \frac{\mathrm{d}\ln(\gamma)}{\mathrm{d}\ln(c_{\mathrm{H}})}\right)^{-1} \tag{16}$$

The factor in brackets is called the thermodynamic factor and can be experimentally measured by the following derivative:

$$\frac{\mathrm{d}U}{\mathrm{d}\ln(c_{\mathrm{H}})} = \frac{RT}{F}\frac{\mathrm{d}\mu_{\mathrm{H}}}{\mathrm{d}\ln(c_{\mathrm{H}})} \tag{17}$$

$$= \frac{RT}{F}\left(1 + \frac{\mathrm{d}\ln(\gamma)}{\mathrm{d}\ln(c_{\mathrm{H}})}\right) \tag{18}$$

Using the tracer diffusion coefficient $D_0$ of a defect-free palladium sample [37], the activity coefficient $\gamma$ can be calculated [39]:

$$\gamma = \frac{D_{\mathrm{H}}}{D_0(1 - c_{\mathrm{H}})^2} \tag{19}$$

At constant EMF, i.e. when hydrogen is evenly distributed throughout the sample, the hydrogen concentration trapped at defects $c_t$ can be estimated with the activity coefficient:

$$c_t = c_{\mathrm{H}}(\gamma - 1) \tag{20}$$

In the case of cold-rolled palladium, where dislocations are the major traps for hydrogen, the trapped hydrogen concentration can also be expressed as follows [7]:

$$c_t = \left[\left(\frac{n_{\mathrm{H}}}{n_{\mathrm{Pd}}}\right)_{deformed} - \left(\frac{n_{\mathrm{H}}}{n_{\mathrm{Pd}}}\right)_{annealed}\right] = \rho\Gamma_{\mathrm{H}}\Omega_{\mathrm{Pd}}, \tag{21}$$

where $\rho$ is the dislocation density, $\Gamma_{\mathrm{H}}$ is the excess amount of hydrogen measured in mol $\mathrm{m}^{-1}$ and $\Omega_{\mathrm{Pd}}$ is the molar volume of palladium with $\Omega_{\mathrm{Pd}} = 8.56 \times 10^{-6}\mathrm{mol/m^3}$ [38]. The comparison of the trapped hydrogen at the same chemical potential $\mu_{\mathrm{H}}$ of two different samples $(A, B)$ allows the relative dislocation density $\rho_A/\rho_B$ to be calculated:

$$c_t = \rho\Gamma(\mu_{\mathrm{H}})\Omega_{\mathrm{Pd}} \tag{22}$$

$$\frac{\rho_A}{\rho_B} = \frac{\rho_A\Gamma(\mu_{\mathrm{H}})\Omega_{\mathrm{Pd}}}{\rho_B\Gamma(\mu_{\mathrm{H}})\Omega_{\mathrm{Pd}}} = \frac{c_{t,A}}{c_{t,B}}. \tag{23}$$

Here, $\Gamma(\mu_{\mathrm{H}})$ is the excess hydrogen, which is an unknown function of the chemical potential of hydrogen $\mu_{\mathrm{H}}$ but is assumed to be independent of the dislocation density, and $\Omega_{\mathrm{Pd}}$ is the molar volume of palladium.

This equation allows one to measure in principle the absolute value of the dislocation density $\rho$ if a reference sample with a known dislocation density is available. The relative dislocation densities were calculated and compared to the results measured with the method of Williamson and Hall [15].

## 4. Results

### 4.1. TEM observations

In this work, the arrangement and the density of dislocations are studied using different methods. Fig. 5a–d shows TEM micrographs of cold-rolled palladium with different hydrogen contents during the cold rolling.

The sample cold rolled in the absence of hydrogen (Fig. 5a) exhibits a few dislocations arranged in dislocation cell walls, with only a small number of dislocations inside the cells. The addition of a small amount of hydrogen (i.e. 0.1 at.% H/Pd) during cold rolling increases the dislocation density and hardly any dislocation cells are observable or at least are very small (Fig. 5b and c). This shows that the global dislocation density increases and the dislocations appear to be distributed homogeneously. The local dislocation density seems not to change as much as the global dislocation density because single dislocations can be seen. By increasing the hydrogen content to 1.0 at.% H/Pd during cold rolling (Fig. 5d), the sample exhibits a cellular structure, with a high dislocation density in the cell

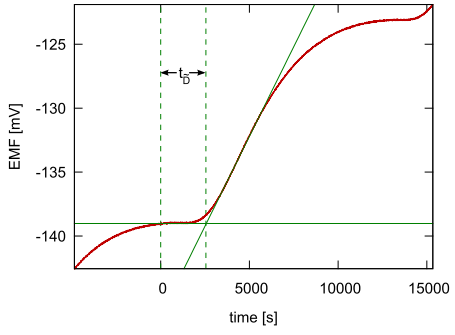


**Fig. 4.** Development of the EMF in the measuring cell. A new electric pulse to load more hydrogen from the loading cell in the sample was initialized at time index 0. When the EMF reaches a new level (here $t = 13300$ s), a new pulse is initialized. The breakthrough time $t_{\mathrm{D}}^{\sim}$ is the time at which a tangent through the point of inflection crosses the EMF level at the starting time ($t = 0$).

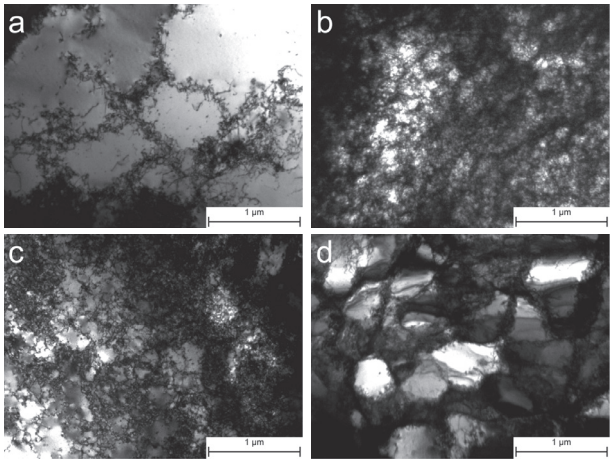


**Fig. 5.** TEM micrographs of cold-rolled palladium without hydrogen (a) and with 0.1 at.% H/Pd (b), 0.5 at.% H/Pd (c) and 1.0 at.% H/Pd (d) during the cold rolling. Reduction in thickness: 50%.

walls and only a few dislocations inside the cells. Furthermore, it can be seen that the individual cells show different contrasts, which is a sign of the formation of subgrains.

### 4.2. Dislocation density of cold-rolled Pd–H alloys by XRD

According to Section 3.1, the dislocation density can be estimated using the method of Williamson and Hall [15]. Table 1 shows the values for the dislocation density for all of the analyzed samples.

### 4.3. The relative dislocation density by diffusion of hydrogen

In order to evaluate the relative dislocation densities as acquired by diffusion measurements, the diffusion coefficient of hydrogen in palladium $D_H$ and the trapped hydrogen $c_t$ must first be analyzed.

$D_H$ was obtained from Eq. (15) via measured values of the breakthrough time $t_D^{\sim}$. The measurement of the diffusion coefficient is also used to measure the amount of trapped hydrogen $c_t$ at crystal defects according to Eqs. (19) and (20). A plot of the tracer diffusion coefficient $D_H$ of hydrogen in palladium vs. the dissolved hydrogen is shown in Fig. 6. It can be seen that the apparent tracer diffusion coefficients of the samples increase with increasing hydrogen content. The tracer diffusion coefficient of the sample which was cold rolled without hydrogen reaches the value of the diffusion coefficient of defect-free material $D_0 = 3.26 \times 10^{-11}$ m$^2$ s$^{-1}$ (293 K [37]) at around 40 atppm H/Pd. The tracer diffusion coefficients of the samples which were cold rolled at higher hydrogen contents reach the value of the tracer diffusion coefficient of defect-free material at higher hydrogen concentrations.

Fig. 7 shows a plot of the trapped hydrogen at crystal defects vs. the chemical potential of hydrogen in palladium. The higher the chemical potential, the greater the amount of hydrogen trapped. Furthermore, it can be seen that samples with higher hydrogen content during cold rolling can trap more hydrogen.

At constant chemical potential $\mu_H = RT\ln(\gamma c_H)$, the relative density $\rho/\rho_{ref}$ is given by $c_t/c_{t,ref}$ (see Eq. (23)), where

**Table 1.** Dislocation density for different samples (columns 2–4) determined by the method of Williamson and Hall [15] of cold-rolled palladium with increasing hydrogen contents during the cold rolling. The labels * and ** correspond to different samples which were also measured by the diffusion method (see Table 2). The numbers in parentheses represent the statistical errors of the last digits.

| H/Pd [at.%] | Dislocation density for different samples ($10^{14}$m/m$^3$) | | |
|---|---|---|---|
| 0.00 | 2.7(3)* | 2.9(1) | |
| 0.10 | 6.1(6)* | | |
| 0.25 | 5.5(5)* | 7.3(8)** | 5.6(4) |
| 0.30 | 7.1(9) | | |
| 0.40 | 8.0(5)* | | |
| 0.50 | 8.4(1)* | 8.0(6)** | 6.2(3) |
| 0.60 | 9.8(9)* | | |
| 0.70 | 9.5(5)* | | |
| 0.75 | 12(1)* | 14(2) | 8.5(3) |
| 0.80 | 9.1(7) | 9.7(5) | |
| 0.90 | 12.5(9) | | |
| 1.00 | 12(2) | | |
| 1.10 | 15(2) | | |
| 1.20 | 12.0(3) | 14.6(6) | |

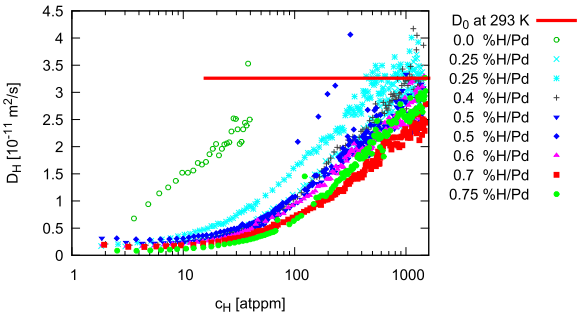


**Fig. 6.** Tracer diffusions coefficient $D_H$ of hydrogen in cold-rolled palladium vs. the hydrogen concentration $c_H$. $D_0 = 3.26 \times 10^{-11}\ \frac{m^2}{s}$ is the tracer diffusion coefficient of defect-free palladium at 293 K [37].

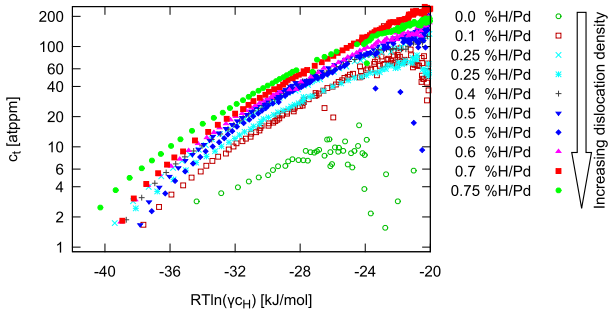


**Fig. 7.** Concentration of the trapped hydrogen $c_t$ at crystal defects in cold-rolled palladium vs.s the chemical potential $\mu_H$ of hydrogen in palladium for samples with different hydrogen contents during deformation.

**Table 2.** Relative dislocation density $\rho/\rho_{ref}$ measured by the diffusion of hydrogen in deformed palladium with different hydrogen contents during cold rolling. The reference specimen labeled "Ref." was deformed with 0.75 at.% H/Pd. The labels * and ** correspond to different samples which were also evaluated by the method of Williamson and Hall (see Table 1). The numbers in parentheses represent the statistical errors of the last digits.

| H/Pd [at.%] | Relative dislocation density $\rho/\rho_{ref}$ |
|---|---|
| 0.00 | 0.14(2)* |
| 0.10 | 0.40(4)* |
| 0.25 | 0.47(2)* |
| 0.25 | 0.65(5)** |
| 0.40 | 0.68(5)* |
| 0.50 | 0.64(8)* |
| 0.50 | 0.74(9)** |
| 0.60 | 0.75(7)* |
| 0.70 | 0.9(2)* |
| 0.75 | 1 (Ref.)* |

$c_{t,ref}$ denotes the trapped hydrogen concentration of a reference sample. The $c_t$ values of a specimen deformed with 0.75 at.% H/Pd were chosen as reference values. The data displayed in Table 2 are the mean values of the relative dislocation densities.

### 4.4. Hydrogen excess at dislocations in palladium

$\Gamma(\mu_H)$ is the excess hydrogen segregated at dislocations in relation to the average hydrogen concentration $c_H = RT\ln(\gamma c_H)$. The independent measurement of the

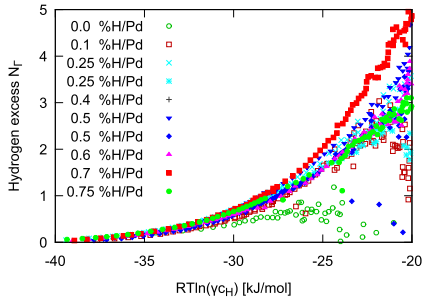


**Fig. 8.** The excess $N_\Gamma$ of hydrogen atoms per Burgers vector at dislocations in cold-rolled palladium vs. the chemical potential of hydrogen in palladium for different deformed palladium samples.

dislocation density $\rho$ with the method of Williamson and Hall allows Eq. (22) to be used to calculate the hydrogen excess at dislocations. To get the absolute number of hydrogen atoms $N_\Gamma$ per Burgers vector $b$, the following relation is used:

$$N_\Gamma = \Gamma(\mu_H) N_A b = \frac{c_t}{\rho \Omega_{Pd}} N_A b \tag{24}$$

where $N_A$ is the Avogadro constant and $\Omega_{Pd}$ is the molar volume of palladium. The excess $N_\Gamma$ vs. the chemical potential $\mu_H$ is shown in Fig. 8. It can be seen that the curve progression is nearly the same for the different cold-rolled samples. The scatter at high hydrogen concentrations can be attributed to inaccuracies of the calculation of the tangent through the point of inflection for the EMF (see Section 3.2): When a constant current pulse is used to increase the hydrogen concentration, the change of the EMF becomes small at higher hydrogen concentrations due to the logarithmic dependency of the EMF on the hydrogen concentration (Eq. (6) and (7)).

## 5. Discussion

The objective of this study was to investigate the influence of hydrogen on the formation and arrangement of dislocations in palladium during cold rolling. For this purpose, hydrogen was loaded electrochemically into well-annealed palladium prior to a cold-rolling process. The remaining hydrogen content was subsequently removed by anodic polarization and the metal sheets were examined by the method of Williamson and Hall [15] and using hydrogen as a probe to quantify the trapped hydrogen concentration at dislocations in palladium via its diffusion coefficient.

### *5.1. Comparison of the different methods to evaluate the dislocation density*

It is well known that hydrogen has a large impact on defect nucleation [2,40,41], defect mobility [17,42] and defect interaction [43,44].

In this study it was shown that, when palladium is cold rolled to a thickness reduction of 50%, the presence of increasing amounts of hydrogen leads to increasing dislocation densities. This behavior is observed by two different methods: the analysis of diffraction patterns of the samples using the method of Williamson and Hall [15] and the analysis of the diffusion time of hydrogen through the palladium samples. XRD measurements showed that a dislocation density of $3 \times 10^{14}$ m$^{-2}$ can be achieved without hydrogen. With the addition of only $0.1 \times 10^{-2} \frac{H}{Pd}$, the dislocation density can be doubled. With further increases in the hydrogen concentration, the dislocation density increases linearly with a slope of $(7.2 \pm 0.8) \times 10^{16}$ m$^{-2} \left(\frac{H}{Pd}\right)^{-1}$.

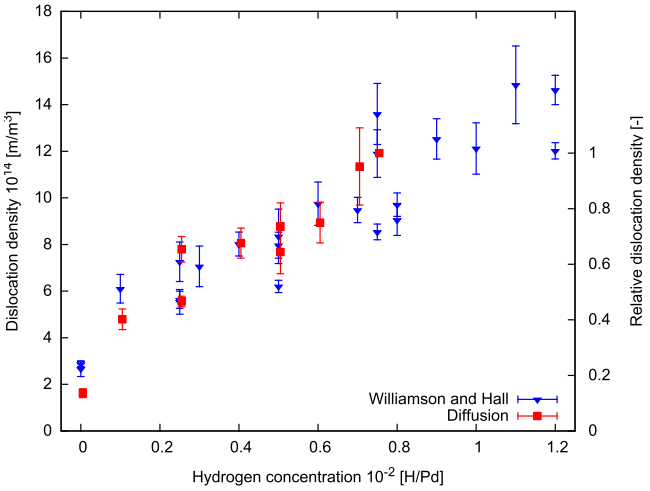


**Fig. 9.** Development of the dislocation density of cold-rolled palladium with increasing hydrogen content during cold rolling. The measurements were performed by two different methods: interpretation of the diffraction patterns of the samples using the method of Williamson and Hall [15] and measurement of the relative dislocation density by evaluating the diffusion time of hydrogen through the palladium samples.

The values for the dislocation density determined by both methods (Tables 1 and 2) are shown in Fig. 9. The scale for the relative dislocation density determined with the diffusion method was chosen so that, at a hydrogen concentration of $0.75 \times 10^{-2} \frac{H}{Pd}$, the relative dislocation density was set to be 1. This shows that the progressions of the dislocation density determined by the two methods are in perfect agreement. Since the two methods show the same results, one can conclude that the assumption that the excess hydrogen $\Gamma(\mu_H)$ per Burgers vector is independent of the dislocation density is justified.

In Fig. 8 the number of excess hydrogen atoms per Burgers vector at dislocations is plotted against the chemical potential of hydrogen $\mu_H = RT \ln(\gamma c_H)$ in the material. As a first approximation, the excess in Fig. 8 falls on the same line. At a higher chemical potential, and accordingly a higher excess, the excess scatters. This could be attributed to dislocation interactions. This means that, for low excess, the hydrogen at dislocations $\Gamma(\mu_H)$ is independent of the dislocation density.

### *5.2. The influence of hydrogen on the dislocation arrangement in cold-rolled palladium–hydrogen alloys*

With the introduction of hydrogen prior to cold rolling, the microstructure of palladium is changed. This can be clearly seen in the TEM pictures (Fig. 5a–d). Without hydrogen, large dislocation cells with small dislocation densities inside the cells are observable. The introduction of a small amount of hydrogen ($0.1 \times 10^{-2} \frac{H}{Pd}$, Fig. 5b) changes the morphology completely: virtually no dislocation cells are observable and the dislocations are more evenly distributed. This is accompanied by a doubling of the dislocation density. This drastic change in dislocation density from pure palladium to palladium with a hydrogen concentration of

$0.1 \times 10^{-2} \frac{H}{Pd}$ during cold rolling also affects the diffusion coefficient of hydrogen in palladium and the amount of hydrogen trapped. The measurements of the palladium–hydrogen alloys show that, with the introduction of a small amount of hydrogen, $0.1 \times 10^{-2} \frac{H}{Pd}$, the dislocation density is doubled compared to the hydrogen-free sample. Without hydrogen during cold rolling, the TEM micrographs of this sample (Fig. 5a) show dislocation cells with only a small number of dislocations inside the cells. The introduction of a small amount of hydrogen ($0.1 \times 10^{-2} \frac{H}{Pd}$; Fig. 5b) during cold rolling changes the global dislocation density and the dislocations appear to be distributed homogeneously. The sample cold rolled with $0.1 \times 10^{-2} \frac{H}{Pd}$ shows no assembly of dislocations in a cell structure. This might be a result of the stabilization of kinks and edge-like parts of dislocations due to the presence of hydrogen. This can be interpreted as the whole line energy of a bent dislocation being reduced by hydrogen. During deformation, this might allow dislocations to bend around obstacles like other dislocations, leading to homogeneously distributed dislocations throughout the whole material.

By further increasing the hydrogen content, refined dislocation cells are observed after cold rolling, together with a decrease in the dislocation density inside the cells. This leads to thicker and denser dislocation cell walls and finally, at higher hydrogen concentrations ($1.0 \times 10^{-2} \frac{H}{Pd}$, Fig. 5d), to the formation of subgrains.

### 5.3. The influence of the dislocation density on hydrogen diffusion

The apparent diffusion coefficient of hydrogen as a function of the hydrogen concentration in palladium for different hydrogen concentrations during cold rolling is shown in Fig. 6. At low hydrogen concentrations, attractive interstitial positions around defects are not saturated by hydrogen. Hydrogen segregating to those sites stays there longer, leading to a longer breakthrough time $t_D^{\sim}$ and a smaller apparent diffusion coefficient [33,34]. With increasing hydrogen content, more hydrogen occupies the remaining unfilled trap sites and therefore the apparent diffusion coefficient increases until it reaches the diffusion coefficient of hydrogen in defect-free palladium. Therefore the apparent diffusion coefficient of the sample which was cold rolled without hydrogen reaches the diffusion coefficient of hydrogen in defect-free palladium with only a small amount of dissolved hydrogen. With increasing dislocation density, a higher hydrogen concentration is needed to saturate the defects. This effect is also shown in the plot of the trapped hydrogen against the total hydrogen concentration (Fig. 7). As expected, an increase in dislocation density leads to more trapped hydrogen.

## 6. Conclusions

In this study, the results of a diffusion-pulse method are presented which were used to evaluate relative dislocation densities. Furthermore, the diffusion coefficient and the excess at dislocations are presented and determined.

The introduction of hydrogen into palladium prior to cold rolling has a large effect on the dislocation density and arrangement. A small amount of hydrogen doubles the dislocation density in comparison to a cold-rolled hydrogen-free sample. Also, the dislocations are distributed homogeneously. With increasing hydrogen content during cold rolling, dislocation cells and finally subgrains are formed.

The results were evaluated based on the defactant concept. The increased dislocation density can be interpreted as a reduction inline energy due to hydrogen; on the other hand, the formation of dislocation cells is regarded as a sign of a reduction in the interaction energy of dislocations, also due to hydrogen.

## Acknowledgements

The authors are grateful for financial support by the Deutsche Forschungsgemeinschaft (KI-230/34).

The authors thank Prof. Dr. Tamás Ungár, from the Department of General Physics, Eötvös University, Budapest, and Dr. May Martin, from the Institut für Materialphysik, Georg-August Universität Göttingen, for fruitful discussions.

## References

[1] P. Rozenak, I.M. Robertson, H.K. Birnbaum, Acta Metall. Mater. 38 (1990) 2031.
[2] D. Pérez Escobar, C. Miñambres, L. Duprez, K. Verbeken, M. Verhaege, Corros. Sci. 53 (2011) 3166.
[3] C.E. Buckley, H.K. Birnbaum, J.S. Lin, S. Spooner, D. Bellmann, P. Staron, et al., J. Appl. Cryst. 34 (2001) 119.
[4] J. Čížek, I. Procházka, S. Daniš, O. Melikhova, M. Vlach, N. Žaludová, et al., Phys. Stat. Sol. C 4 (2007) 3485.
[5] Y. Fukai, Y. Ishii, Y. Goto, K. Watanabe, J. Alloy. Compd. 313 (2000) 121.
[6] R. Kirchheim, Acta Mater. 55 (2007) 5129.
[7] R. Kirchheim, Acta Mater. 55 (2007) 5139.
[8] J. Albrecht, I.M. Bernstein, A.W. Thompson, Met. Mater. Trans. A 13A (1982) 811.
[9] C. Borchers, T. Michler, A. Pundt, Adv. Eng. Mater. 10 (2008) 11.
[10] A.J. West, M.R. Louthan, Met. Mater. Trans. A 10A (1979) 1675.
[11] H.K. Birnbaum, MRS Bull. 28 (2003) 479.
[12] Y.Z. Chen, H.P. Barth, M. Deutges, C. Borchers, F. Liu, R. Kirchheim, Scripta Mater. 68 (2013) 743.
[13] R. Kirchheim, Int. J. Mat. Res. 100 (2009) 483.
[14] M. Maxelon, A. Pundt, W. Pyckhout-Hintzen, J. Barker, R. Kirchheim, Acta Mater. 49 (2001) 2625.
[15] G.K. Williamson, W.H. Hall, Acta Metall. Mater. 1 (1953) 22.
[16] J. Čížek, I. Procházka, F. Bečvář, R. Kužel, M. Cieslar, G. Brauer, et al., Phys. Rev. B 69 (2004) 224106.
[17] P.J. Ferreira, I.M. Robertson, H.K. Birnbaum, Acta Metall. Mater. 46 (1998) 1749.
[18] Y.Z. Chen, A. Herz, Y.J. Li, C. Borchers, P. Choi, D. Raabe, et al., Acta Mater. 61 (2013) 3172.
[19] J.W. Gibbs, Trans. Conn. Acad. 3 (1876) 108.
[20] T. Tabata, H.K. Birnbaum, Scripta Metall. Mater. 17 (1983) 947.
[21] I.M. Robertson, H.K. Birnbaum, Acta Metall. Mater. 34 (1986) 353.
[22] H.K. Birnbaum, P. Sofronis, Mater. Sci. Eng. A 176 (1994) 191.
[23] J.P. Hirth, J. Lothe, Theory of Dislocations, McGraw-Hill, New York, 1968.
[24] D.L. Holt, J. Appl. Phys. 41 (1970) 3197.
[25] D.L. Holt, Sec. Int. Conf. Strength of Metals and Alloys (1970) 477.
[26] P. Hähner, Acta Mater. 44 (1996) 2345.
[27] M. Wilkens, Phys. Status. Solidi. A 2 (1970) 359.
[28] I. Groma, T. Ungár, M. Wilkens, J. Appl. Cryst. 21 (1988) 47.

[29] T. Ungár, G. Tichy, Phys. Stat. Sol. A 171 (1999) 425.
[30] G.K. Williamson, R.E. Smallman, Philos. Mag. 1 (1956) 34.
[31] N. Boes, H. Züchner, J. Less-common Met. 49 (1976) 223.
[32] R. Kirchheim, Acta Metall. Mater. 29 (1981) 835.
[33] R. Kirchheim, U. Stolz, J. Non-Cryst. Solids 70 (1985) 323.
[34] R. Kirchheim, Prog. Mater. Sci. 32 (1988) 261.
[35] H. Züchner, Z. Naturforsch 25a (1970) 1490.
[36] H. Züchner, H.-G. Schöneich, J. Less-common Met. 101 (1984) 363.
[37] J. Vökl, H. Wipf, Hyperfine Interact. 8 (1981) 631.
[38] C.N. Singman, J. Chem. Educ. 61 (1984) 137.
[39] R. Kirchheim, Phys. Scripta T 94 (2001) 58.
[40] A. Barnoush, H. Vehoff, Acta Mater. 58 (2010) 5274.
[41] Y. Katz, N. Tymiak, W.W. Gerberich, Eng. Fract. Mech. 68 (2001) 619.
[42] A. Barnoush, M. Asgari, R. Johnsen, Scripta Mater. 66 (2012) 414.
[43] N. Kheradmand, J. Dake, A. Barnoush, H. Vehoff, Philos. Mag. 92 (2012) 3216.
[44] M. Deutges, I. Knorr, C. Borchers, C.A. Volkert, R. Kirchheim, Scripta Mater. 68 (2013) 71.